

Non variability of intervening absorbers observed in the UVES spectra of the “naked-eye” GRB080319 ^{*}

V. D’Elia^{1,2†}, F. Fiore¹, P. Goldoni^{3,4}, V. D’Odorico⁵, S. Campana⁶, S. Covino⁶,
P. D’Avanzo⁶, E.J.A. Meurs^{7,8}, L. Norci⁸, G. Tagliaferri⁶

¹ *INAF-Osservatorio Astronomico di Roma, Via Frascati 33, I-00040 Monteporzio Catone, Italy;*

² *ASI-Science Data Centre, Via Galileo Galilei, I-00044 Frascati, Italy;*

³ *Laboratoire Astroparticule et Cosmologie, 10 rue A. Domon et L. Duquet, 75205 Paris Cedex 13, France;*

⁴ *Service d’Astrophysique, DSM/DAPNIA/Sap, CEA-Saclay, 91191 Gif-sur-Yvette, France;*

⁵ *INAF, Osservatorio Astronomico di Trieste, Via Tiepolo 11, 34143 Trieste, Italy;*

⁶ *INAF, Osservatorio Astronomico di Brera, via E. Bianchi 46, 23807 Merate (LC), Italy;*

⁷ *School of Cosmic Physics, DIAS, 31 Fitzwilliam Place, Dublin 4, Ireland;*

⁸ *School of Physical Sciences and NCPST, DCU, Glasnevin, Dublin 9, Ireland;*

Accepted... Received...; in original form...

ABSTRACT

The aim of this paper is to investigate the properties of the intervening absorbers lying along the line of sight of Gamma-Ray Burst (GRB) 080319B through the analysis of its optical absorption features. To this purpose, we analyze a multi-epoch, high resolution spectroscopic observations ($R=40000$, corresponding to 7.5 km s^{-1}) of the optical afterglow of GRB080319B ($z = 0.937$), taken with UVES at the VLT. Thanks to the rapid response mode (RRM), we observed the afterglow just 8m:30s after the GRB onset when the magnitude was $R \sim 12$. This allowed us to obtain the best signal-to-noise, high resolution spectrum of a GRB afterglow ever (S/N per resolution element ~ 50). Two further RRM and target of opportunity observations were obtained starting 1.0 and 2.4 hours after the event, respectively. Four MgII absorption systems lying along the line of sight to the afterglow have been detected in the redshift range $0.5 < z < 0.8$, most of them showing a complex structure featuring several components. Absorptions due to FeII, MgI and MnII are also present; they appear in four, two and one intervening absorbers, respectively. One out of four systems show a MgII $\lambda 2796$ rest frame equivalent width larger than 1 \AA . This confirms the excess of strong MgII absorbers compared to quasars, with $dn/dz = 0.9$, ~ 4 times larger than the one observed along quasar lines of sight. In addition, the analysis of multi-epoch, high-resolution spectra allowed us to exclude a significant variability in the column density of the single components of each absorber. Combining this result with estimates of the size of the emitting region, we can reject the hypothesis that the difference between GRB and QSO MgII absorbers is due to a different size of the emitting regions.

Key words: gamma-rays: bursts – ISM: abundances – line: profiles – atomic data.

1 INTRODUCTION

Intervening metal absorption lines have routinely been observed along the line of sight to quasars (QSOs). Among these features, strong MgII $\lambda 2796$, $\lambda 2803$ absorption doublets (with equivalent width $EW > 0.3 \text{ \AA}$) represent good

indicators of metal-enriched gas associated with foreground galaxies. This is because Magnesium is an α element produced by red giants and dispersed in the interstellar medium (ISM) by supernovae and stellar winds (Bergeron & Boisse 1991, Steidel et al. 1994). In particular, such a strong doublet on a QSO sightline witnesses the presence of $0.1 - 5L_*$ galaxies within 60 kpc projected distance and with different morphological types (Churchill et al. 2005, Kacprzak et al. 2008). In addition, the $EW > 1 \text{ \AA}$ MgII intervening absorbers are hosted within dark matter halos with characteristic masses of $10^{11} - 10^{12} M_\odot$ (Bouche’ et al. 2006) and

^{*} Based on observations collected at the European Southern Observatory, ESO, the VLT/Kueyen telescope, Paranal, Chile, in the framework of programs 080.A-0398

[†] E-mail: delia@mporzio.astro.it

$\sim 80\%$ are associated with Damped Lyman-alpha systems (DLAs, Rao et al. 2006).

For a few hours after their onset, Gamma-Ray Burst (GRB) afterglows are the brightest beacons in the far Universe: therefore they provide an alternative and complementary way to QSOs to fully explore the properties of high- z galaxies in which they are hosted (see Savaglio 2006; Prochaska et al. 2007) and of those along their sightlines. In principle, the sightlines of QSOs and GRBs are expected to be equivalent. Prochter et al. (2006) found ~ 7000 strong ($EW > 1\text{\AA}$) MgII intervening absorbers in ~ 50000 QSO spectra from the SDSS DR4, which corresponds to a redshift number density of $dn/dz = 0.24$. Surprisingly, the same authors report the identification of 14 MgII systems along 14 GRB sightlines, which translates into a redshift number density of $dn/dz = 0.90^{+0.83}_{-0.50}$ (99% confidence interval), almost 4 times higher than the QSO one. On the other hand, the intervening CIV absorbers for the two classes of sources do not show any statistical difference (Sudilovsky et al. 2007, Tejos et al. 2007).

The reason for this discrepancy is still uncertain, and several scenarios have been widely discussed (see e.g. Porciani et al. 2007 and Cucchiara et al. 2009). One of these interpretations requires a different size of the source, namely, that QSO emitting regions are larger than GRBs which in turn are comparable to the typical size of the MgII clouds (Frank et al. 2007). In this scenario variability in the column densities of the MgII absorber is expected, since the Lorentz factor decreases because the fireball decelerates on the interstellar medium, and thus the GRB emission regions increase. A MgII variability in multi-epoch spectroscopy data on GRB060206 was first claimed by the analysis by Hao et al. (2007), but then disproved by Aoki et al. (2008) and Thöne et al. (2008).

Occasionally, extremely bright optical transient emission is associated with the GRB event, offering the superb opportunity to take spectra of the afterglows with high resolution instruments. In a fraction of these cases, multi-epoch, high resolution spectroscopy with an adequate signal to noise ratio (S/N) can be obtained, allowing to make detailed studies of the host galaxy ISM and to put strong constraints on its physical parameters (see Vreeswijk et al. 2007 for GRB060418, and D’Elia et al. 2009a for GRB080319B). Here we take advantage of the high quality data collected for GRB083019B to make a systematic study of this GRB sightline and to search for variability of the MgII intervening absorbers.

The paper is organized as follows. Section 2 presents a short summary of the GRB080319B detection and observations; Section 3 describes the datasets and data reduction; Section 4 presents the full analysis of the intervening systems identified in the spectra; finally in Section 5 the results are discussed and conclusions are drawn.

2 GRB080319B

GRB080319B was discovered by the Burst Alert Telescope (BAT) instrument on board Swift on 2008, March 19, at 06:12:49 UT. Swift slewed to the target in less than 1 minute and a bright afterglow was found by both the X-Ray Telescope (XRT) and UV-Optical Telescope (UVOT) at RA =

14h 31m 40.7s, Dec = $+36^\circ 18' 14.7''$ (Racusin et al. 2008a) with observations starting 60.5 and 175 s after the trigger, respectively.

The field of GRB080319B was imaged by the "Pi of the Sky" apparatus located at Las Campanas Observatory before, during and after the GRB event (Cwiok et al. 2008). The field was also targetted by the robotic telescope REM just 43 s after the BAT trigger (Covino et al. 2008a, b). The TORTORA wide-field optical camera (12 cm diameter, 20×25 deg FOV, TV-CCD, unfiltered) mounted on REM also imaged the field before, during and after the GRB event with good temporal resolution (Karpov et al. 2008). These observations show that the GRB reached the magnitudes $V = 5.3$ about 20 s and $H = 4.2$ about 50 s after the trigger. This makes GRB080319B the brightest GRB ever recorded at optical wavelengths (Racusin et al. 2008b, Bloom et al. 2009).

3 OBSERVATIONS AND DATA REDUCTION

We observed the bright afterglow of GRB080319B in the framework of the ESO program 080.A-0398 with the VLT/UVES (Dekker et al. 2000). The Observation Log and the setups used are reported in Table 1. Both UVES dichroics, as well as the red and the blue arms, were used.

The first, 10min observation, was performed in Rapid Response Mode (RRM) and started just 8m:30s after the GRB event, when the afterglow was extremely bright ($R_{Mag} = 12 - 13$). This provided a S/N=30 – 50 per resolution element. Two more UVES observations followed, the first one was again in RRM mode, activated in the framework of program 080.D-0526 and starting 1.0 hours after the GRB event. The second one was a Target of Opportunity (ToO), starting 2.4 hours after the GRB, see Table 1. A slit width of $1''$ has been used in all the observations; this corresponds to a spectral resolution of $R = 40000$, or 7.5 km s^{-1} .

Data reduction was carried out by using the UVES pipeline (Ballester et al. 2000). The final useful spectra extend from $\sim 3800 \text{\AA}$ to $\sim 9500 \text{\AA}$. The spectra were normalized to the continuum, which was evaluated by fitting the data with cubic splines, after the removal of the absorption features. Finally, the noise spectrum, used to determine the errors on the best fit line parameters, was calculated from the real, background-subtracted spectra using line-free regions. This takes into account both statistical and systematic errors in the pipeline processing and background subtraction.

4 THE GRB080319B SIGHTLINE

An analysis of the GRB080319B UVES spectra reveals at least 5 absorbing systems along the GRB line of sight. The presence of excited FeII and NiII features in the higher redshift system is a clear indication that its gas belongs or is close to the host galaxy of the GRB. We will not discuss the host galaxy absorber, since a detailed study has been reported by D’Elia et al. (2009a); but instead we will now concentrate on the intervening systems.

The four intervening absorbers identified have redshifts

Table 1. GRB080319B journal of observations and setups used

Obs	UT observation	T. from burst (s)	Setup (nm)	Wavelength (Å)	Slit	Resolution	Exp. (s)	S/N	R mag
RRM 1	2008 Mar 19, 06:21:26	517	Dic 2, 437	3760 - 4980	1"	40000	600	~ 30	12 - 13
RRM 1	2008 Mar 19, 06:21:26	517	Dic 2, 860	6700 - 10430	1"	40000	600	~ 50	12 - 13
RRM 2	2008 Mar 19, 07:18:47	3441	Dic 1, 346	3040 - 3870	1"	40000	1800	~ 7	16 - 17
RRM 2	2008 Mar 19, 07:18:47	3441	Dic 1, 580	4780 - 6810	1"	40000	1800	~ 12	16 - 17
RRM 2	2008 Mar 19, 08:06:42	6833	Dic 2, 437	3760 - 4980	1"	40000	1800	~ 7	16 - 17
RRM 2	2008 Mar 19, 08:06:42	6833	Dic 2, 860	6700 - 10430	1"	40000	1800	~ 12	16 - 17
ToO	2008 Mar 19, 08:43:52	8546	Dic 1, 346	3040 - 3870	1"	40000	1200	~ 5	16 - 17
ToO	2008 Mar 19, 08:43:52	8546	Dic 1, 580	4780 - 6810	1"	40000	1200	~ 8	16 - 17
ToO	2008 Mar 19, 09:07:18	10478	Dic 2, 437	3760 - 4980	1"	40000	1200	~ 5	16 - 17
ToO	2008 Mar 19, 09:07:18	10478	Dic 2, 860	6700 - 10430	1"	40000	1200	~ 8	16 - 17

in the range 0.5 – 0.8. Each system features MgII absorption. FeII, MgI and MnII are also present; they appear in four, two and one intervening absorbers, respectively. The analysis of these systems is often intricate due to the complexity of the absorption lines of the spectrum, which in several cases cannot easily be fit with a single line profile. The presence of several components is indicative of clumpy gas in the intervening absorbers, similarly to what observed for the circumburst environment of many GRBs (See e.g., D’Elia et al. 2007, Piranomonte et al. 2009, D’Elia et al. 2009a,b) and for the MgII intervening absorbers along the QSO sightlines (Churchill & Vogt 2001). Whenever a system can not be fit by a single line profile, it can be interpreted both as a clumpy system with a complex velocity structure or as many systems lying at different redshifts. This is why we say that GRB080319B has at least four intervening systems. We arbitrarily chose to consider as a single system two or more absorption features closer than 500 km s⁻¹. Tab. 2 summarizes the characteristics of the intervening absorbers. Column 2 gives the heliocentric redshift, column 3 the absorbing elements and ions, column 4 the total width of the system, column 5 the rest frame equivalent width (EW_{r,f}) of the MgIIλ2796 line, column 6 the number of components necessary to adequately fit each system. The intervening absorbers are ordered with decreasing redshift. For multiple component systems the *z* reference values have been arbitrarily placed to be coincident with the component indicated in column 7; for single component absorbers the redshift is defined by the best fit value of the central absorption line wavelength.

The next subsections report the analysis for each intervening absorber. The fitting procedure for the absorption systems has been carried out as follows. First of all, we analyzed the first epoch spectrum, that with the highest signal-to-noise ratio. The spectrum was analyzed in the MIDAS environment using the FITLYMAN procedure (Fontana & Ballester 1995). The line profile fitting is usually performed using a Voigt function. Each Voigt profile has basically three free parameters: the central wavelength of the transition, the column density of the absorbing species and the doppler parameter *b* of the gas. A single component treatment is often inadequate, reflecting the complexity of the intervening systems, as noted before. We thus fit the data several times with different numbers of components, in order to minimize the reduced χ^2 values. MgII, which appears in all systems, is the one with a larger velocity spread,

so it was used to guide the identification of all components. The other species, when present, allowed us to best constrain the central wavelength positions in the regions where the MgII results to be strongly saturated. The central wavelengths and the *b* parameters have been kept fixed among the different species, unless otherwise stated. Once a satisfactory fit to the first epoch spectrum was obtained, we turned to the analysis of the other two epochs. Again, the central wavelengths and the *b* parameters were fixed to the first epoch results. To increase the S/N of the later epoch observations, we added them (the second and third spectra) and repeated the fits to the coadded spectrum. Tables 3 to 6 report the results of our analysis for the intervening absorbers 1 to 4, respectively. In particular, column 2 shows the number of features contributing to the fit for each species, column 3 reports the epoch to which the data refers, and the following ones the column densities of each component for that specific element or ion. Components are identified with progressive numbers for decreasing redshifts (or decreasing wavelengths, i.e., the higher the wavelength or the positive velocity shift, the lower the component number). Errors are the formal 1 σ uncertainties given by FITLYMAN; upper limits have the 90% level confidence.

4.1 The intervening system 1

This is the system with the lowest number of absorption features. In fact, only the MgII λ2796, λ2803 doublet and the FeII λ2382 line are present at *z* = 0.76046. Despite this, the structure of the system, which spans a velocity range of ~ 90 km s⁻¹ is quite complex, and a four component model is necessary in order to obtain a reasonable fit to the data. Fig. 1 shows the absorption due to the MgII doublet and the FeII λ2382 line, together with the results of the four component fit. The FeII λ2382 line is only present in the fourth component of the first observation. The S/N ratio of the following observations just allows to set upper limits for this feature. Table 3 reports the column densities for each component. We can rule out a variability of both the MgII and FeII lines, since all the column densities are consistent within the 2 σ level.

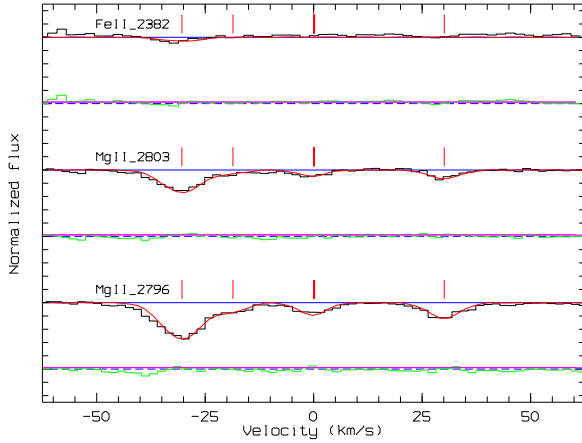
The non variability of the MgII features is also shown in Fig. 2, which displays the MgII λ2796 features for the three epochs.

Table 2. Absorption systems along the GRB080319B sightline

System	redshift	species	Width (km s ⁻¹)	MgII $\lambda 2796$ EW _{rf} * (Å)	# of components	z reference component
1	0.76046	MgII, FeII	90	0.121 ± 0.007	4	2nd
2	0.71468	MgII, MgI, FeII	400	1.448 ± 0.007	10	7th
3	0.56578	MgII, FeII	30	0.083 ± 0.006	1	1st
4	0.53035	MgII, MgI, FeII, MnII	100	0.62 ± 0.01	6	3rd

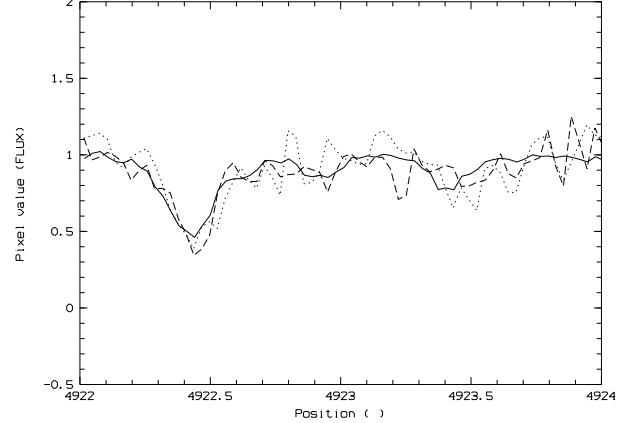
* Rest frame values, errors are at 1 σ confidence level.**Table 3.** Column densities for the absorption system 1

Species	Trans.	Obs.	I (+30 km s ⁻¹)	II (0 km s ⁻¹)	III (-20 km s ⁻¹)	IV (-30 km s ⁻¹)
Mg II	$\lambda 2796$	1	11.83 ± 0.02	11.91 ± 0.16	10.56 ± 0.07	12.37 ± 0.01
		2	11.75 ± 0.09	< 11.7	< 11.7	12.33 ± 0.04
		3	< 12.1	< 12.1	< 12.1	12.22 ± 0.07
		2+3	11.72 ± 0.08	< 11.7	< 11.7	12.29 ± 0.03
Fe II	$\lambda 2382$	1	< 11.5	< 11.5	< 11.5	11.53 ± 0.09
		2	< 12.7	< 12.7	< 12.7	< 12.7
		3	< 13.1	< 13.1	< 13.1	< 13.1
		2+3	< 12.7	< 12.7	< 12.7	< 12.7

All values are logarithmic cm⁻²**Figure 1.** The MgII $\lambda 2796$, $\lambda 2803$ absorption doublet and the FeII $\lambda 2382$ line of the first intervening system, for the first epoch spectrum. Solid lines represent our four Voigt components, best fit model. Vertical lines identify the velocity of each component with respect to the zero point arbitrarily placed at $z = 0.76046$ and coincident with component II.

4.2 The intervening system 2

This is the most complex system, which spans the largest velocity range (~ 400 km s⁻¹). A lot of absorption features are present at the redshift of 0.71468, namely: the MgII $\lambda 2796$, $\lambda 2803$ doublet, MgI ($\lambda 2852$) and FeII in several flavours ($\lambda 2344$, $\lambda 2374$, $\lambda 2382$, $\lambda 2586$ and $\lambda 2600$). The first epoch spectrum required a ten component fit in order to obtain a good modeling to the data. Fig. 3 shows the absorption due to the MgII doublet and MgI $\lambda 2852$, while Fig. 4 displays all the features of FeII; in both figures the results of the ten component fit are also plotted. Table 4 reports the column densities for each component. No variability is detected in

**Figure 2.** A comparison between the MgII $\lambda 2796$ optical depth in the three UVES observation epochs, for the first intervening system. Solid line refers to the first epoch spectrum (8m30s after the Swift trigger), dashed line to the second epoch spectrum (1.0 hours after the GRB event), and dotted line to the third epoch spectrum (2.4 hours after the GRB event).

the three epochs within the 3σ uncertainty. This rules out column density variability for the intervening system 2. The only exception is represented by the second component of the MgII. Anyway, this specific component is strongly saturated, so the values reported in the corresponding column of Table 4 may not be entirely reliable.

The non variability of the features belonging to the second system can also be seen in Figs. 5-7, which display the MgII $\lambda 2796$, MgI $\lambda 2852$ and FeII $\lambda 2600$ features for the three epochs, respectively. This system is the only one showing an $EW_{MgII,rf} > 1$ so we also computed the EWs of the absorption features for comparison with other works. The

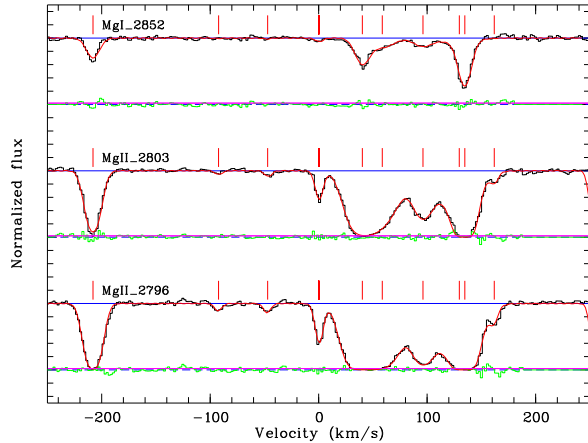


Figure 3. The MgII $\lambda 2796$, $\lambda 2803$ doublet and the MgI $\lambda 2852$ feature of the second intervening system, for the first epoch spectrum. Solid lines represent our ten Voigt components, best fit model. Vertical lines identify the velocity of each component with respect to the zero point arbitrarily placed at $z = 0.71468$ and coincident with component VII.

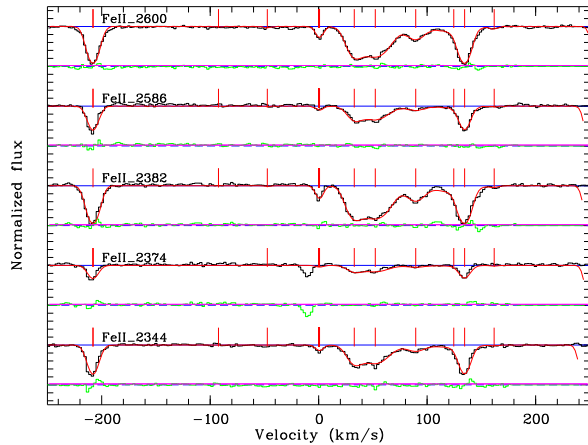


Figure 4. All the FeII features of the second intervening system, for the first epoch spectrum. Solid lines represent our ten Voigt components, best fit model. Vertical lines identify the velocity of each component with respect to the zero point arbitrarily placed at $z = 0.71468$ and coincident with component VII.

MgII $\lambda 2796$ EW does not vary between the three observations at the 2σ confidence level, and a variability of this feature, if present, is less than 10% at the 3σ confidence level. The FeII $\lambda 2600$ and MgI $\lambda 2852$ rest frame EWs are $EW_{FeII,rf} = 0.708 \pm 0.007$ and $EW_{MgI,rf} = 0.289 \pm 0.007$, respectively (1σ confidence). These values are not different from that observed along other GRB sightlines (see e.g. Cucchiara et al. 2009).

4.3 The intervening system 3

This is the simplest system among the intervening absorbers. Its velocity dispersion is just $\sim 30 \text{ km s}^{-1}$ and only two ions appear in the spectrum at the redshift of $z = 0.56578$: MgII, with the classical $\lambda 2796$, $\lambda 2803$ doublet and FeII ($\lambda 2586$ and

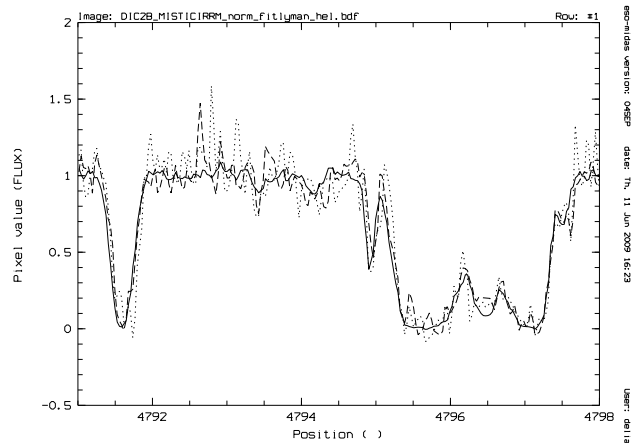


Figure 5. A comparison between the MgII $\lambda 2796$ optical depth in the three UVES observation epochs, for the second intervening system. Solid line refers to the first epoch spectrum (8m30s after the Swift trigger), dashed line to the second epoch spectrum (1.0 hours after the GRB event), and dotted line to the third epoch spectrum (2.4 hours after the GRB event).

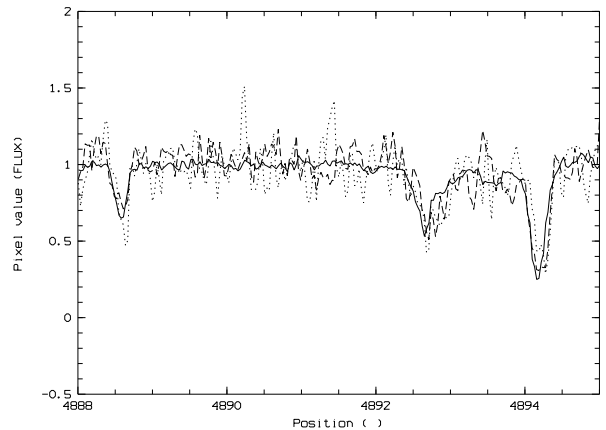


Figure 6. A comparison between the MgI $\lambda 2852$ optical depth in the three UVES observation epochs, for the second intervening system. Solid line refers to the first epoch spectrum (8m30s after the Swift trigger), dashed line to the second epoch spectrum (1.0 hours after the GRB event), and dotted line to the third epoch spectrum (2.4 hours after the GRB event).

$\lambda 2600$). All the three epoch spectra are well fit by a single component Voigt profile. Fig. 8 shows the absorption from the MgII and FeII features, together with our fit to the data. Table 5 reports the column densities measured for the three epochs. We can rule out a variability of both MgII and FeII lines, since the column densities of the three epochs are consistent within the 3σ level.

The non variability of the features belonging to the third system is also shown in Figs 9 and 10, which display the MgII $\lambda 2796$ and FeII $\lambda 2600$ features for the three epochs, respectively.

Table 4. Column densities for the absorption system 2

Species	Trans.	Obs.	I (160 km s ⁻¹)	II (135 km s ⁻¹)	III (125 km s ⁻¹)	IV (90 km s ⁻¹)	V (50 km s ⁻¹)	
			VI (30 km s ⁻¹)	VII (0 km s ⁻¹)	VIII (-50 km s ⁻¹)	IX (-100 km s ⁻¹)	X (-210 km s ⁻¹)	
Mg II	λ2796	1	13.84 ± 0.05	15.45 ± 0.08	13.05 ± 0.02	13.04 ± 0.02	13.29 ± 0.02	
		2	13.79 ± 0.12	16.01 ± 0.06	13.03 ± 0.04	13.07 ± 0.13	13.32 ± 0.04	
	λ2803	3	< 12.2	14.83 ± 0.12	13.07 ± 0.04	13.21 ± 0.19	13.19 ± 0.11	
		2+3	13.57 ± 0.16	15.11 ± 0.30	13.24 ± 0.06	12.99 ± 0.04	13.19 ± 0.08	
		1	13.65 ± 0.02	12.57 ± 0.03	12.66 ± 0.49	12.56 ± 0.34	13.44 ± 0.03	
		2	13.64 ± 0.12	12.50 ± 0.06	12.37 ± 0.28	13.03 ± 1.95	13.57 ± 0.05	
		3	13.56 ± 0.10	12.37 ± 0.09	< 12.1	12.27 ± 0.64	13.53 ± 0.04	
		2+3	13.70 ± 0.07	12.43 ± 0.06	< 11.9	12.78 ± 0.23	13.54 ± 0.05	
	Mg I	λ2852	1	< 10.5	12.18 ± 0.01	11.19 ± 0.07	11.29 ± 0.03	11.45 ± 0.03
			2	< 11.2	12.10 ± 0.04	< 11.2	< 11.2	11.29 ± 0.11
3			< 11.6	12.10 ± 0.03	< 11.6	< 11.6	< 11.6	
2+3			< 11.2	12.08 ± 0.05	11.34 ± 0.14	< 11.2	11.13 ± 0.12	
		1	11.77 ± 0.01	10.63 ± 0.09	< 10.5	< 10.5	11.45 ± 0.03	
		2	11.77 ± 0.04	< 11.2	< 11.2	< 11.2	11.49 ± 0.06	
		3	11.75 ± 0.03	< 11.6	< 11.6	< 11.6	< 11.6	
		2+3	11.78 ± 0.05	< 11.2	< 11.2	< 11.2	11.58 ± 0.05	
FeII		λ2344, λ2374	1	13.33 ± 0.08	13.43 ± 0.01	12.40 ± 0.03	12.68 ± 0.01	13.40 ± 0.02
			2	13.79 ± 0.18	13.35 ± 0.04	12.52 ± 0.09	12.64 ± 0.04	13.43 ± 0.02
	3		13.44 ± 0.56	13.39 ± 0.06	< 12.7	12.80 ± 0.05	13.42 ± 0.03	
	2+3		13.77 ± 0.17	13.35 ± 0.03	12.53 ± 0.08	12.71 ± 0.03	13.41 ± 0.02	
		1	13.15 ± 0.01	12.35 ± 0.02	< 11.7	< 11.7	13.48 ± 0.01	
		2	13.09 ± 0.04	< 12.4	< 12.4	< 12.4	13.40 ± 0.04	
		3	13.12 ± 0.05	< 12.7	< 12.7	< 12.7	13.43 ± 0.05	
		2+3	13.12 ± 0.08	12.18 ± 0.08	< 12.1	< 12.1	13.41 ± 0.03	

All values are logarithmic cm⁻²**Table 5. Column densities for the absorption system 3**

Species	Trans.	Obs.	I (0 km s ⁻¹)
Mg II	λ2796	1	12.73 ± 0.02
		2	12.57 ± 0.05
	λ2803	3	12.71 ± 0.09
		2+3	12.63 ± 0.05
Fe II	λ2586	1	12.40 ± 0.04
		2	12.28 ± 0.18
	λ2600	3	< 12.7
		2+3	12.18 ± 0.15

All values are logarithmic cm⁻²

4.4 The intervening system 4

This is the system which shows the greatest number of species. Three ions, MgII (λ2796, λ2803), FeII (λ2586, λ2600), MnII (λ2576, λ2594) and the neutral MgI (λ2852) appear in the spectrum at the redshift of $z = 0.53035$. The velocity dispersion of the system is ~ 100 km s⁻¹. Since both MgII features are strongly saturated, we used MgI and FeII to guide the identification of the components. The spectrum around these features results to be well fit by a six component model. Fig. 11 shows the absorptions from the MgII and MgI features, while Fig. 12 those from FeII and MnII. These figures also display our six component fit to the data. Table 6 reports the column densities measured for the three

epochs divided by components. Variability can be excluded for MgI, FeII and MnII whose components are consistent in the three epochs within the 3σ uncertainty. MgII seems not to behave this way, but most of the components of its features are strongly saturated, so the corresponding column density values reported in the table are less reliable. Components 1 and 6 are not saturated (the former is not saturated only in the MgII λ2803 feature), and they are consistent with no variability within the 3σ uncertainty. It is worth noting, however, that component 6 has a positive detection in the first observation only, while in the other epochs just upper limits can be set. Saturation is also present in component 2 and 3 of the FeII, but just in the first observation.

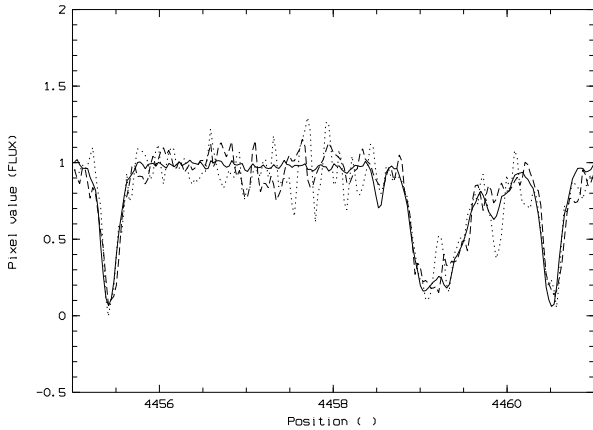


Figure 7. A comparison between the FeII $\lambda 2600$ optical depth in the three UVES observation epochs, for the second intervening system. Solid line refers to the first epoch spectrum (8m30s after the Swift trigger), dashed line to the second epoch spectrum (1.0 hours after the GRB event), and dotted line to the third epoch spectrum (2.4 hours after the GRB event).

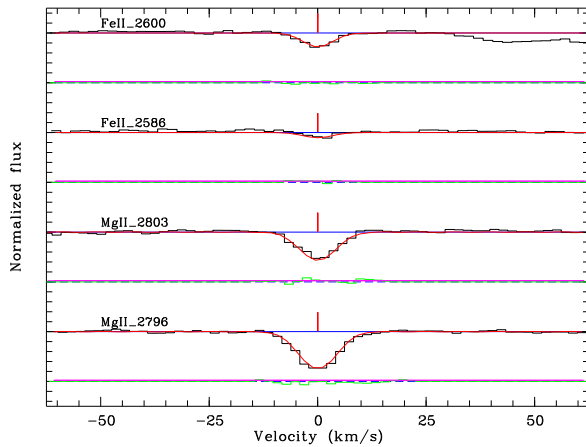


Figure 8. The MgII $\lambda 2796$, $\lambda 2803$ doublet and the FeII $\lambda 2586$, $\lambda 2600$ absorption features of the third intervening system, for the first epoch spectrum. Solid lines represent our Voigt profile, best fit model. The vertical line identifies the position of the central wavelength of the voigtian.

The non variability of the features belonging to the fourth system is also shown in Figs. 13-15, which display the MgII $\lambda 2796$, MgI $\lambda 2852$ and FeII $\lambda 2600$, features for the three epochs, respectively.

5 CONCLUSIONS

In this paper we present high resolution ($R=40000$, corresponding to 7.5 km/s) spectroscopy of the optical afterglow of the “naked-eye” Gamma Ray Burst GRB080319B ($z = 0.937$), observed by UVES at the VLT in three different epochs, starting ~ 8.30 minutes, ~ 1 and ~ 2.4 hours after the trigger, respectively.

We concentrate here on the intervening absorbers along

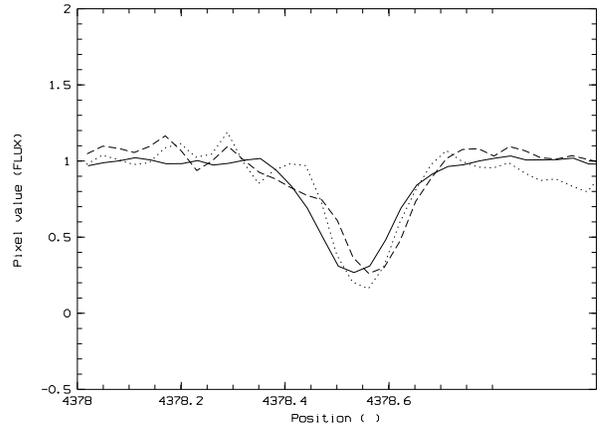


Figure 9. A comparison between the MgII $\lambda 2796$ optical depth in the three UVES observation epochs, for the third intervening system. Solid line refers to the first epoch spectrum (8m30s after the Swift trigger), dashed line to the second epoch spectrum (1.0 hours after the GRB event), and dotted line to the third epoch spectrum (2.4 hours after the GRB event). The slight wavelength shift of the second and third epoch spectra with respect to the first one ($\sim 0.04\text{\AA}$ or < 3 km/s, lower than the spectral resolution, see also fig. 10) is possibly an offset that comes out from the data reduction and not a real effect.

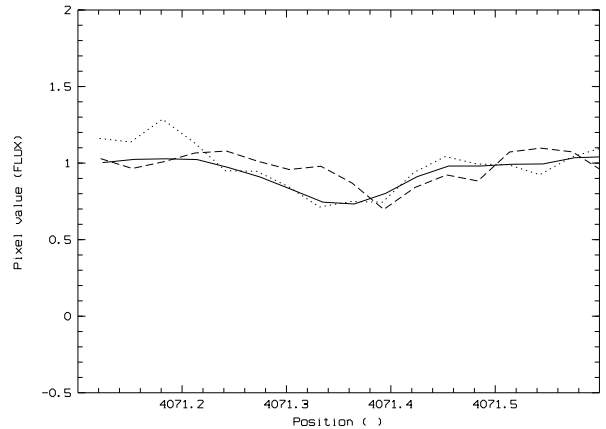
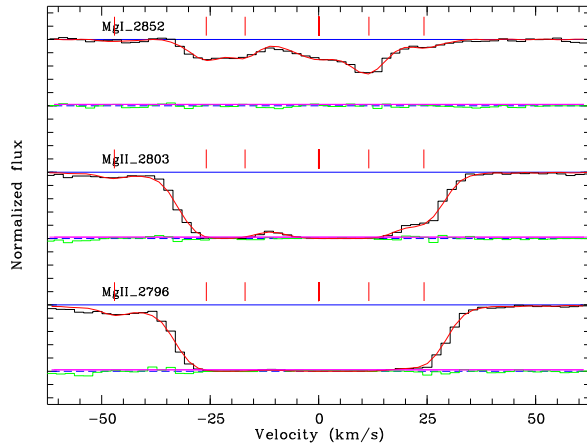
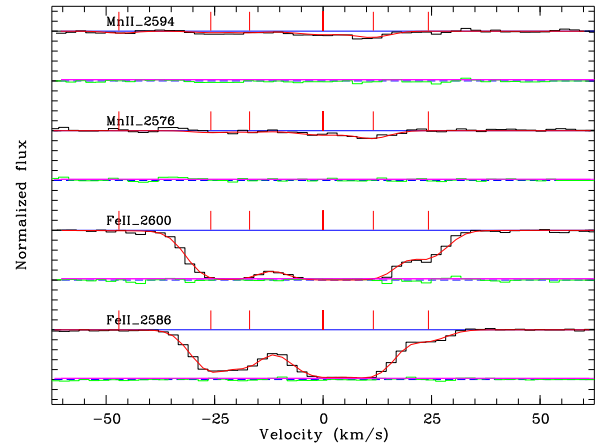


Figure 10. A comparison between the FeII $\lambda 2600$ optical depth in the three UVES observation epochs, for the third intervening system. Solid line refers to the first epoch spectrum (8m30s after the Swift trigger), dashed line to the second epoch spectrum (1.0 hours after the GRB event), and dotted line to the third epoch spectrum (2.4 hours after the GRB event).

the GRB sightline, since the absorption features in the vicinity of the afterglow have already been studied and presented in D’Elia et al. (2009a). Our spectral coverage allows to analyze a redshift path for the MgII $\lambda 2796$ in the range $z = 0.36 - 0.937$. We are sensitive to lines with EW down to 0.015 (at the 2σ confidence level), thanks to the extremely high S/N of the first RRM observation. At least four intervening systems between $z = 0.8$ and $z = 0.5$ have been identified. Most of them show a complex structure constituted by several components, similar to that of the intervening absorbers along the QSO sightlines (Churchill & Vogt 2001).

Table 6. Column densities for the absorption system 4

Species	Trans.	Obs.	I (25 km s ⁻¹)	II (10 km s ⁻¹)	III (0 km s ⁻¹)	IV (-15 km s ⁻¹)	V (-25 km s ⁻¹)	VI (-50 km s ⁻¹)	
Mg II	λ2796	1	12.94 ± 0.02	15.00 <i>S</i> ± 0.15	15.25 <i>S</i> ± 0.04	13.22 <i>S</i> ± 1.71	14.61 <i>S</i> ± 0.04	11.40 ± 0.04	
	λ2803	2	12.75 ± 0.09	15.24 <i>S</i> ± 0.56	16.13 <i>S</i> ± 0.15	15.68 <i>S</i> ± 0.22	13.02 <i>S</i> ± 0.22	< 11.9	
		3	12.79 ± 0.10	15.81 <i>S</i> ± 0.06	14.75 <i>S</i> ± 0.13	14.94 <i>S</i> ± 0.12	13.91 <i>S</i> ± 0.18	< 12.1	
		2+3	12.71 ± 0.08	15.93 <i>S</i> ± 0.07	13.83 <i>S</i> ± 0.16	15.39 <i>S</i> ± 0.24	13.91 <i>S</i> ± 0.17	< 11.8	
Mg I	λ2852	1	11.17 ± 0.06	12.48 ± 0.09	11.67 ± 0.03	11.44 ± 0.03	11.45 ± 0.48	10.82 ± 1.86	
		2	< 11.2	11.96 ± 0.30	11.64 ± 0.08	11.67 ± 0.08	< 11.2	< 11.2	
		3	< 11.5	12.96 ± 0.42	11.79 ± 0.09	11.53 ± 0.13	< 11.5	< 11.5	
		2+3	< 11.1	13.02 ± 0.80	11.71 ± 0.07	11.59 ± 0.07	< 11.1	< 11.1	
Fe II	λ2586	1	12.80 ± 0.06	15.74 <i>S</i> ± 0.09	14.38 <i>S</i> ± 0.09	13.65 ± 0.07	13.51 ± 0.15	< 11.8	
		λ2600	2	12.75 ± 0.10	13.67 ± 0.47	14.03 ± 0.13	13.68 ± 0.17	13.75 ± 0.50	< 12.3
			3	12.85 ± 0.23	15.06 ± 0.81	14.09 ± 0.36	13.69 ± 0.24	13.33 ± 0.24	< 12.5
			2+3	12.81 ± 0.12	14.33 ± 0.60	14.05 ± 0.16	13.67 ± 0.19	13.54 ± 0.49	< 12.2
Mn II	λ2576	1	< 11.4	11.80 ± 0.03	11.78 ± 0.03	11.56 ± 0.16	< 11.4	< 11.4	
		λ2594	2	< 12.4	< 12.4	< 12.4	< 12.4	< 12.4	< 12.4
			3	< 12.7	< 12.7	< 12.7	< 12.7	< 12.7	< 12.7
			2+3	< 12.2	< 12.2	< 12.2	< 12.2	< 12.2	< 12.2

All values are logarithmic cm⁻²**Figure 11.** The MgII λ2796, λ2803 doublet and the MgI λ2852 absorption features of the fourth intervening system, for the first epoch spectrum. Solid lines represent our six component, best fit model. Vertical lines identify the velocity of each component with respect to the zero point arbitrarily placed at $z = 0.53035$ and coincident with component III.**Figure 12.** The FeII λ2586, λ2600 and the MnII λ2576, λ2594 absorption features of the fourth intervening system, for the first epoch spectrum. Solid lines represent our six component, best fit model. Vertical lines identify the velocity of each component with respect to the zero point arbitrarily placed at $z = 0.53035$ and coincident with component III.

All systems feature the MgII λ2796, λ2803 doublet. FeII, MgI and MnII lines are detected in four, two and one systems, respectively.

Prochter et al. (2006) claimed that the incidence of strong MgII absorbers along GRB sight lines is nearly four times higher than that along the line of sight to QSOs. They analyzed the spectra of 14 GRB optical afterglows, finding on average one intervening system per afterglow with equivalent width $> 1 \text{ \AA}$. The GRB080319B sightline confirms this trend, since the rest frame EW of the MgII λ2796 absorption line is $> 1 \text{ \AA}$ in one system.

Structured intervening systems are expected if the discrepancy between QSOs and GRBs intervening absorbers is due to a different size of the source, namely, if QSO emitting regions are larger than GRBs which in turn are comparable

to the typical size of the MgII clouds (Frank et al. 2007). According to their estimation, the QSO beam size must be larger than $3 \times 10^{16} \text{ cm}$ while for the GRB beam they suggest a size around a few $\times 10^{15} \text{ cm}$. To observe this effect, the MgII absorber should then be patchy with a clump size around 10^{16} cm . Nevertheless, in this scenario, variability in the column densities of the MgII absorbers along the GRB sightlines is expected. MgII variability in multi-epoch spectroscopy data on GRB060206 was first claimed by the analysis by Hao et al. (2007), but then disproved by Aoki et al. (2008) and Thöne et al. (2008). This work confirms the lack of variability in the column densities of the GRB intervening absorbers, in the specific case of GRB080319B. In particular, the EW of the MgII λ2796 absorption line is consistent within 2σ in the three UVES observations. Given

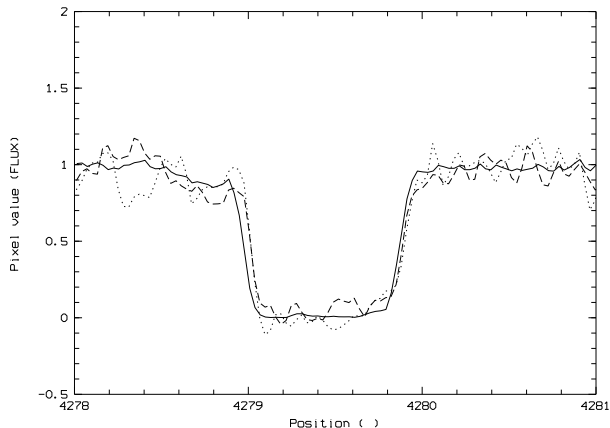


Figure 13. A comparison between the MgII $\lambda 2796$ optical depth in the three UVES observation epochs, for the fourth intervening system. Solid line refers to the first epoch spectrum (8m30s after the Swift trigger), dashed line to the second epoch spectrum (1.0 hours after the GRB event), and dotted line to the third epoch spectrum (2.4 hours after the GRB event). The $\sim 0.04\text{\AA}$ frequency shift (see also figs. 14 and 15) is present also in this system, confirming that its nature is not physical, but due to the reduction process.

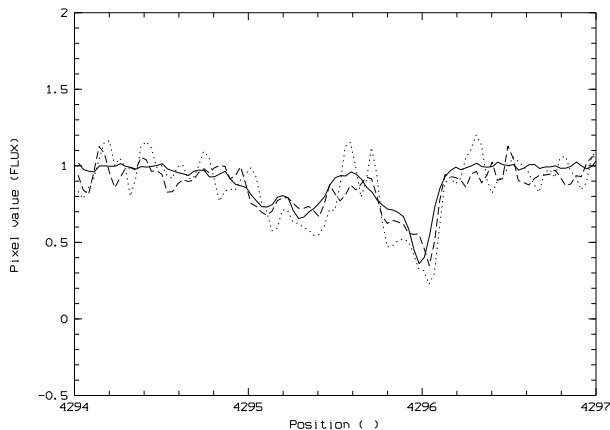


Figure 14. A comparison between the MgI $\lambda 2852$ optical depth in the three UVES observation epochs, for the fourth intervening system. Solid line refers to the first epoch spectrum (8m30s after the Swift trigger), dashed line to the second epoch spectrum (1.0 hours after the GRB event), and dotted line to the third epoch spectrum (2.4 hours after the GRB event).

the S/N ratio of our data, we can conclude that a variability of this feature, if present, is less than 10% at the 3σ confidence level. This upper limit is three times smaller than the ones that can be estimated for GRB060206 using the data by Aoki et al. (2008). Racusin et al. (2008b) modeled the radiation of GRB080319B as coming from a structured jet constituted by an inner, narrow jet ($\theta_n = 0.2^\circ$) and an outer, wider jet ($\theta_w = 4^\circ$). They interpreted the optical emission at $T < T_0 + 800$ s (T_0 being the burst detection time) as produced by the reverse shock of the inner jet, while that at $T > T_0 + 800$ as the signature of the forward shock of the outer jet. Since the first UVES observation starts at

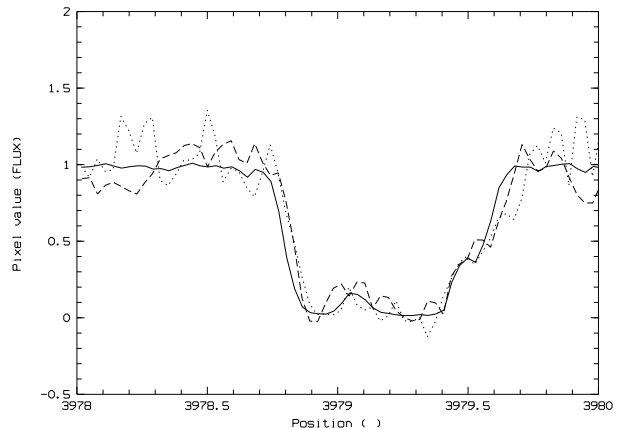


Figure 15. A comparison between the FeII $\lambda 2600$ optical depth in the three UVES observation epochs, for the fourth intervening system. Solid line refers to the first epoch spectrum (8m30s after the Swift trigger), dashed line to the second epoch spectrum (1.0 hours after the GRB event), and dotted line to the third epoch spectrum (2.4 hours after the GRB event).

$T \sim T_0 + 500$ while the second and the third ones start more than 1hr later, a strong increase in the size of the emitting region is expected from this scenario. In more detail, the dimension of the emitting region is $\sim 10^{17}$ cm at the beginning of the GRB event and $\sim 10^{18}$ cm a few hours later (Pandey et al. 2009, Racusin et al. 2008b and Kumar & Panaitescu 2008). Although we cannot be more quantitative, a variation of a factor of ten in the dimension of the emitting region would imply a considerable reduction of the intervening column densities, but it is not detected. Indeed, time resolved, high resolution spectroscopy allows us for the first time to exclude a significant ($> 3\sigma$) variability even by considering the single components of each intervening system alone.

Porciani et al. (2007) investigated several possible explanations for the strong MgII excess, namely, dust obscuration bias, clustering of the absorbers, different beam sizes of the sources, multiband magnification bias of GRBs, association of the absorbers with the GRB event or with the circumburst environment. They concluded that none of these effects alone can explain the observed difference, but maybe the combination of two or more of them can reduce the significance of the discrepancy. We can take advantage of the dimensions of the emitting source in GRB080319B and the lack of variability in the intervening absorbers to characterize the absorbers along this GRB sightline. Since these dimensions are in the range $10^{17} - 10^{18}$ cm, the MgII (and other species) clouds cannot have clumps or structures smaller than 0.1 – 1 pc, otherwise we should observe variability in their absorption. This is not obvious, since Ding et al. (2003) show that smaller intervening absorbers are present along the line of sight to QSOs.

Cucchiara et al. (2009) compared 81 QSOs and 6 GRB lines of sight obtained with UVES. They found no significant evidence to support a difference between the two absorber populations, concluding that a possible explanation for the MgII excess could be intrinsic to the GRB environment. A similarity between the narrow lines of the GRB intervening absorbers and that produced by the material ejected in the

accretion disk winds of QSOs has been pointed out. Nevertheless, the high velocities required by the intervening redshifts ($v/c \sim 0.2 - 0.4$) and the lack of fine structure features in these systems represent a strong weakness of this picture. In addition, Tejos et al. (2009) recently found no evidence for a similar excess considering the weak ($0.07 < EW < 1\text{\AA}$) MgII systems along the line of sight of 8 GRB observed with echelle spectrographs. These authors tend to exclude an intrinsic nature of the discrepancy, since it would result in an excess in the weak systems too. They suggest that the best explanation available at present could be gravitational lensing bias due to lensing by the host galaxy of the absorber. Indeed the strong MgII system along the GRB080319B sightline has a velocity of ~ 36300 km/s with respect to the GRB. The data do not show evidence either of broad profiles and/or partial coverage (see e.g. D'Odorico et al. 2004), so this absorber is likely an intervening system.

Combining the data by Prochter et al. (2006) with the results from the analysis in this paper and that in D'Elia et al. (2009b) regarding the line of sight to GRB080330, we obtain 16 strong ($EW > 1\text{\AA}$) MgII intervening absorbers along 16 GRB sightlines. The total redshift path becomes 17.02, and this results in a $dn/dz = 0.94$. This surprising excess of strong MgII absorbers with respect to QSO sightlines remains a matter of debate and a satisfactory explanation is still missing. Clearly more observations and analysis are needed in order to solve this issue.

REFERENCES

- Aoki, K., Totani, T., Hattori, T. et al., 2008, PASJ, in press, arXiv:08084157
- Ballester, P., Modigliani, A., Boitquin, O., et al.: 2000, ESO Messenger, 101, 31
- Bergeron, J. & Boisse, P. 1991, A&A, 243, 344
- Bloom, J.S., Perley, D.A., Li, W. et al. 2008, ApJ, 691, 723
- Bouche', N., Murphy, M.T., Peroux, C., Csabai, I. & Wild, V., 2006, MNRAS, 371, 495
- Churchill, C.W. & Vogt, S.S., 2001, AJ, 122, 679
- Churchill, C.W., Kacprzak, G.G. & Steidel, C.C., 2005, in IAU Colloq. 199, Probing Galaxies through Quasar Absorption Lines, ed. P.R. Williams, C. Shuu & B. Menard (Cambridge: Cambridge Univ. Press), 24
- Covino, S. et al., 2008a, GCN 7431
- Covino, S. et al., 2008b, GCN 7446
- Cucchiara, A. et al. 2008, GCN 7547
- Cucchiara, A., Jones, T., Charlton, J. C., Fox, D. B., Einsig, D. & Narayanan, A., 2009, ApJ, 693, 345
- Cwiok, M. et al. 2008, GCN 7439
- Dekker, H., D'Odorico, S., Kaufer, A., Delabre, B., Kotzłowski, H., 2000, SPIE, 4008, 534D
- D'Elia, V., Fiore, F., Meurs, E.J.A. et al., 2007, A&A 467, 629
- D'Elia, V., Fiore, F., Perna, R. et al., 2009a, ApJ in press, arXiv:08042141
- D'Elia, V., Fiore, F., Perna, R. et al., 2009b, accepted by A&A
- Ding, J., Charlton, J.C., Bond, N.A., Zonak, S.G.; Churchill, C.W. 2003, ApJ, 587, 551
- D'Odorico, V., Cristiani, S., Romano, D., Granato, G., Danese, L., 2004, MNRAS, 351, 976
- Frank, S., Bentz, M.C., Stanek, K.Z., Mathur, S. Dietrich, M., Peterson, B.M. & Atlee, D.W., 2007, Ap&SS 312 325
- Hao, H., Stanek, K.Z., Dobrzycki, A. et al., 2007, ApJ, 659, 99
- Kacprzak, G.G., Churchill, C.W., Steidel, C.C. & Murphy, M.T., 2008, AJ, 135, 922
- Karpov et al. 2008, GCN 7452
- Kumar, P., Panaitescu, A., 2008, MNRAS, 391, 19L
- Pandey, S.B., Castro-Tirado, A.J., Jelinek, M. et al., 2009, Accepted for publication in A&A, arXiv0904.1797
- Piranomonte, S., Ward, P.A., Fiore, F. et al. 2008, A&A, 492, 775
- Porciani, C., Viel, M. & Lilly, S.J., 2007, ApJ, 659, 218
- Prochaska J.X., Chen, H.W., Dessauges-Zavadsky, M. & Bloom, J.S., 2007, ApJ, 666, 267
- Prochter, G.E., Prochaska, J.X., Chen, H.-W. et al. 2006, ApJ, 648, L930
- Rao, S.M., Turnshek, D.A. & Nestor, D.B., 2006, ApJ, 636, 610
- Racusin, J.L. et al. 2008a GCN 7427
- Racusin, J.L., Karpov, S.V., Sokolowski, M. et al., 2008b, Nature, 455, 183
- Savaglio, S., 2006, New J. Phys, 8, 195
- Steidel, C.C., Dickinson, M. & Persson, S.E., 1994, ApJ, 437, L75
- Steidel, C.C., Adelberger, K.L., Giavalisco, M., Dickinson, M., Pettini, M. 1999, ApJ, 519, 1
- Sudilovsky et al. 2007, ApJ, 669, 741
- Tejos, N., Lopez, S., Prochaska, J.X., Chen, H.-W. & Dessauges-Zavadsky, M., 2007, ApJ, 671, 622
- Tejos, N., Lopez, S., Prochaska, J.X., Bloom, J.S., Chen, H.-W., Dessauges-Zavadsky, M., Maureira, M.J., 2009, ApJ submitted, arXiv0905.3768
- Thöne, C.C., Wiersema, K., Ledoux, C. et al. 2008, A&A, 489, 37
- Vreeswijk, P.M., Ledoux, C., Smette, A. et al. 2007, A&A, 468, 83